Rheo-optical Raman study of microscopic deformation in high-density polyethylene under hot drawing

Rheo-optical Raman study of microscopic deformation in high-density polyethylene under hot drawing

Takumitsu Kida, Yusuke Hiejima*, Koh-hei Nitta

Department of Chemical and Materials Science, Kanazawa University

Kakuma Campus, Kanazawa 920-1192, Japan

**Corresponding author:*

Department of Chemical and Materials Science, Kanazawa University, Kakuma Campus, Kanazawa, 920-1192, Japan. Tel.: +81 76 264 6256 E-mail: hiejima@se.kanazawa-u.ac.jp (Yusuke Hiejima)

Abstract

In situ observation of the microscopic structural changes in high-density polyethylene during hot drawing was performed by incorporating a temperature-controlled tensile machine into a Raman spectroscopy apparatus. It was found that the load sharing and molecular orientation during elongation drastically changed at 50°C. The microscopic stress of the crystalline chains decreased with increasing temperature and diminished around 50°C. Moreover, the orientation of the crystalline chains was greatly promoted above 50°C. These microscopic structural changes were caused by the thermal activation of the molecular motion within lamellar crystalline chains owing to the onset of relaxation of the crystalline phase.

Keywords: High-density polyethylene; *In situ* Raman spectroscopy; Hot drawing

1. Introduction

The mechanical properties of semicrystalline polymers, such as polyethylene (PE), drastically change with temperature, which are accompanied by at least three relaxations: including α, β, and γ relaxations [1]. The α relaxation of high-density polyethylene (HDPE) occurs in a wide range of temperature from 30 to 120°C, and the activation energy varies from 90 to 300 kJ/mol [1–3]. Nakayasu *et al.* reported that the α relaxation in HDPE can be divided into two relaxations: α_1 and α_2 at low and high temperatures, respectively [4]. They reported the activation energies as ~117 kJ/mol for the α_1 relaxation and ~210 kJ/mol for the α_2 relaxation. The α_1 and α_2 relaxations were assigned as relaxation in the grain boundaries and the thermal activation of the intrachain motion, respectively. These assignments were confirmed by dynamic mechanical analysis (DMA) of PE single-crystal mats [5] and PE with different molecular weight distributions and branch structures [6]. Because molecular motion is activated in the α relaxation region, the drawability of polymeric materials is highly enhanced. Thus, most films and fibers are commonly produced at high temperatures.

The effect of α relaxation on the deformation of semicrystalline polymeric materials has been investigated by various methods, such as DMA, nuclear magnetic resonance and X-ray diffraction, mainly using highly drawn specimens [5,7,8]. Jiang *et al.* [9] conducted *in situ* small- and wide-angle X-ray measurements of PE under hot drawing. They found that the long period drastically decreases with strain in the neck-formation region below 100°C, while the long period remains unchanged with elongation above

120°C. However, investigations by *in situ* measurements, which can directly observe the deformation mechanism, are very limited.

Because α relaxation is due to inter- or intracrystalline relaxation, drastic changes in molecular mobility occur under hot drawing. Rheo-optical techniques, such as infrared (IR) absorption and Raman scattering, are suitable to elucidate the microscopic mechanism of deformation [10–14]. Although IR spectroscopy has been applied to hot drawing of thin films [15,16], this method has several intrinsic disadvantages, such as most IR active modes being mainly ascribed to vibrations of side chains, and only the orientation parameter $\langle P_2 \rangle$, which is a measure of the average orientation degree, can be determined. However, Raman spectroscopy has several advantages over IR spectroscopy, such as the skeletal C–C stretching vibration being strongly Raman active, load sharing on the polymer chains can be directly observed [17], and the higher-order orientation parameter $\langle P_4 \rangle$ can be estimated. Then, by using Raman spectroscopy, we can discuss the molecular orientation more precisely [18–21]. In this work, Raman spectra of HDPE were monitored under tensile stretching at high temperatures in a range of the α-relaxation processes. To accomplish this, we mounted a small tensile machine with a heat chamber on a Raman spectroscopic system.

2. Experimental

In this study, we used Ziegler–Natta-catalyzed HDPE ($M_w = 10 \times 10^4$, $M_n = 1.7 \times 10^4$) supplied by Tosoh Corporation. A sheet of HDPE about 1 mm thick was prepared by a hot-press method, where the pellets were melt and compressed at 210°C for 5 min at 20 MPa followed by quenching in iced water. The sample sheet was annealed at 110°C for 5 h. The test specimens for the measurements were cut from the annealed

film with a double-edge-notched die (2-mm gauge length and 4-mm width). The density of the sample was determined to be 953 kg/m^3 by the Archimedes method. The volumetric crystallinity was determined to be 68% by assuming that the density of the amorphous and the crystalline phases were 855 and 1000 kg/m^3 [22], respectively. The lamellar thickness of the sample was determined to be about 17 nm by SAXS measurements.

Dynamic mechanical spectra were measured from −50°C to 140°C at a constant frequency of 10 Hz and a heating rate of 2 °C/min using a UBM DVE-V4 dynamic mechanical analyzer (UBM, Kyoto, Japan). As shown in Fig. 1, one broad relaxation peak was observed, which was identified conventionally as α (overlapping α_1 and α_2). The α_1 and α_2 processes were observed at 62 and 121°C, respectively.

A schematic of the apparatus for the *in situ* Raman spectroscopic measurements for hot drawing is shown in Fig. 2. A temperature-controlled tensile machine for microscopy (10073B, Japan High Tech Co. Ltd.) was installed in the *in situ* Raman spectroscopy apparatus that we recently developed [23]. The laser light from a He–Ne laser (LASOS) was monochromated with a laser line filter, and irradiated into the notched portion of the specimen with a spot size of 1 mm in diameter. The elongation speed was set to 1 mm/min and the drawing temperature was tuned from 20 to 80°C. The scattered light was collected with a concave mirror and collimated with a convex lens into an optical fiber, and the excitation light was removed with a Raman long-pass filter. An intensified charge-coupled device camera equipped with a monochromator (PIXIS100 and SpectraPro 2300i, Princeton Instruments) was used as the detector. For polarized Raman spectroscopy, a pair of wire-grid polarizers was inserted as the polarizer and the analyzer. The non-polarized spectra were accumulated 10 times with

an exposure time of 1 or 2 s. The polarized spectra were collected in *zz*, *yz*, and *yy* geometries and accumulated 10 times with an exposure time of 2 s.

The C–C stretching modes of PE are strongly Raman active [24–27]. The anti-symmetric (1063 cm^{-1}) and symmetric (1130 cm^{-1}) stretching modes correspond to vibrations of carbon atoms along and perpendicular to the molecular chain, respectively. The experimental Raman spectra in the C–C stretching region (1050–1150 cm^{-1}) were successfully fitted with a sum of two Voigt functions using the nonlinear Levenberg–Marquardt method, and the peak positions and peak areas for the two peaks were determined [23]. The uncertainties in determining the peak shifts and the peak areas were less than ±0.22 cm^{-1} and ±5% (except at 80°C, less than ±10%), respectively.

The peak shifts of the symmetric and anti-symmetric vibrations were defined as the deviation of the Raman shifts from that of the undrawn specimens:

$$\Delta\nu_{s} = \nu_{s} - \nu_{s}^{0}, \tag{1}$$

$$\Delta\nu_{as} = \nu_{as} - \nu_{as}^{0}, \tag{2}$$

where the superscript 0 denotes the undrawn specimens. From the direction of the symmetric and anti-symmetric vibrations, $\Delta\nu_{s}$ and $\Delta\nu_{as}$ were interpreted as the microscopic stresses perpendicular and parallel to the polymer chain, respectively.

The orientational behavior of the polymer chain was evaluated with the orientation parameters obtained by polarized Raman spectroscopy [18–21,28]. The orientation parameters $\langle P_2 \rangle$ and $\langle P_4 \rangle$ are defined as a function of the chain orientation angle θ with respect to the draw axis as

$$\langle P_2 \rangle = \frac{3\langle \cos^2\theta \rangle - 1}{2}, \tag{3}$$

$$\langle P_4 \rangle = \frac{35\langle \cos^4\theta \rangle - 30\langle \cos^2\theta \rangle + 3}{8}. \tag{4}$$

The values of $\langle P_2 \rangle$ and $\langle P_4 \rangle$ were evaluated from the integrated intensities of the 1130 cm^{-1} band in the polarized spectra [18,19,23,29,30]. The polar angle distribution of the polymer chains is described by the orientation distribution function (ODF, $N(\theta)$). For Raman spectroscopy, the expression of the ODF is given by [19–21]

$$N(\theta) = \frac{1}{2} + \frac{5}{2}\langle P_2 \rangle P_2(\theta) + \frac{9}{2}\langle P_4 \rangle P_4(\theta) \,. \tag{5}$$

The most probable distribution function ($\langle P_4 \rangle_{mp}$) is calculated under the assumption of the maximum entropy for a given value of $\langle P_2 \rangle$ [18–20]. The analytical forms of $\langle P_4 \rangle_{mp}$ are given by

$$\langle P_4 \rangle_{mp} = -0.083\langle P_2 \rangle + 1.366\langle P_2 \rangle^2 - 1.899\langle P_2 \rangle^3 + 1.616\langle P_2 \rangle^4 \tag{6}$$

for positive $\langle P_2 \rangle$, and

$$\langle P_4 \rangle_{mp} = 0.052\langle P_2 \rangle + 1.574\langle P_2 \rangle^2 + 3.968\langle P_2 \rangle^3 + 8.058\langle P_2 \rangle^4 \tag{7}$$

for negative $\langle P_2 \rangle$ [20].

3. Results and Discussion

In situ Raman spectra of HDPE at a strain of 10 for various drawing temperatures are shown in Fig. 3. The assignments of the corresponding Raman bands are shown in Table 1. While the Raman bands at 1063, 1298, 1440, and 1460 cm^{-1} are insensitive to temperature, the bands at 1130 (trans chain) and 1418 cm^{-1} (crystalline) do depend on temperature. The intensities of the latter two bands increase with temperature, because the molecular orientation owing to elongation is enhanced at higher temperatures.

The stress–strain curves at elevated temperatures are shown by the solid curves in Fig. 4. The first yield because of initiation of the collapse of spherulites and the second yield because of the onset of neck formation [31–34] are clearly observed at $\varepsilon \approx 0.6$ and $\varepsilon \approx$

1.1, respectively. The overall stress, including the first yield stress, drastically decreases with increasing temperature. While each stress–strain curve has a sharp peak at the first yield point in the leather-like region (<50°C), the peak becomes broader and the second yielding is more clearly observed in the α_1 relaxation region (>50°C). Because the shape of stress–strain curves is sensitive to the deformation mechanism of the polymeric materials [35,36], drastic changes are expected in the microscopic structure of HDPE during hot drawing.

In Fig. 4, the peak shifts of the symmetric ($\Delta\nu_s$) and anti-symmetric ($\Delta\nu_{as}$) C–C stretching modes are plotted against applied strain. In the elastic region, $\Delta\nu_s$ and $\Delta\nu_{as}$ remain about zero, which suggests no stress is applied to the polymer chains in the crystalline phase. $\Delta\nu_{as}$ shows a downward deviation around the first yield point, which suggests an increase of the stretching stress along the polymer chain. At 20°C, $\Delta\nu_{as}$ sharply decreases at the first yielding point, while the slope is more gradual above 50°C. The strain dependence of $\Delta\nu_s$ in the yielding region shows a clear difference between the leather-like region and the α_1 relaxation region: $\Delta\nu_s$ shows a prominent peak around the second yielding point at 20°C, while $\Delta\nu_s$ remains close to zero above 50°C. Compression stress is then applied perpendicular to the polymer chain in the leather-like region, while almost no stress is applied in the α_1 relaxation region. The heterogeneous load sharing (stretching along the polymer chain and compression perpendicular to the chain) in HDPE during cold drawing has been interpreted by the stress concentration during neck formation, where the densification of lamellar clusters occurs [23]. The heterogeneous load sharing in the yielding region is shown by Fig. 5, where $\Delta\nu_s$ and $\Delta\nu_{as}$ are plotted against temperature for $\varepsilon = 1.1$. The positive $\Delta\nu_{as}$ and negative $\Delta\nu_s$ below 50°C are a direct consequence of the heterogeneous load sharing. The

microscopic stress in both directions decreases with increasing temperature, and both $\Delta\nu_{as}$ and $\Delta\nu_{s}$ are about zero above 50°C. The decrease of the microscopic stress can be explained as follows. Because the increase of E'' begins at around 20°C (see Fig. 1), intercrystalline relaxation starts to occur above room temperature, and is enhanced at higher temperatures. The onset of intercrystalline motion may make the stacked lamellar cluster units, which are the origin of the heterogeneous load sharing [23], more mobile in the yielding process. The stress on the crystalline chain is greatly reduced above 50°C, suggesting that the stress is concentrated on the amorphous chains. In the strain-hardening region, $\Delta\nu_{s}$ and $\Delta\nu_{as}$ gradually decrease with increasing strain. Under large deformation ($\varepsilon \approx 10$), the value of $\Delta\nu_{s}$ is appreciably larger than that of $\Delta\nu_{as}$. This might be because of formation of fibrillar structures, where $\Delta\nu_{s}$ is twice as large as $\Delta\nu_{as}$ [17].

The orientation parameters $\langle P_2 \rangle$ and $\langle P_4 \rangle$ at various drawing temperatures are plotted against strain in Fig. 6. The stress–strain curves are also shown in Fig. 6 for comparison. While $\langle P_2 \rangle$ remains zero in the elastic region, $\langle P_2 \rangle$ begins to increase after the first yield point, and the slope of $\langle P_2 \rangle$ increases around the second yield point. In the strain-hardening region, the slope of $\langle P_2 \rangle$ becomes gradual, and $\langle P_2 \rangle$ approaches an asymptotic value which increases with increasing temperature. Because $\langle P_2 \rangle$ is a measure of the average degree of orientation of the molecular chain, molecular orientation begins after the first yield, accelerates around the second yield point, proceeds gradually in the strain-hardening region and, finally, highly orientated fibrous states are achieved. This orientational behavior is consistent with previous studies [10–14]. Above 50°C, the strain dependence of $\langle P_4 \rangle$ is similar to that of $\langle P_2 \rangle$, and the value of $\langle P_4 \rangle$ is very close to $\langle P_4 \rangle_{mp}$. Then, molecular orientation in the α_1 relaxation region

should be entropically favorable; the average direction of molecular orientation is represented by the value of $\langle P_2 \rangle$, and polymer chains are smoothly distributed with respect to the average direction [18–20]. At 20°C, $\langle P_4 \rangle$ starts to decrease around the second yield point, and reaches a minimum after the second yield point. The downward deviation of $\langle P_4 \rangle$ from $\langle P_4 \rangle_{mp}$ has been explained by the steric hindrance of the bulky lamellar cluster units [23]. The minimum value of $\langle P_4 \rangle$ during drawing is plotted against temperature in Fig. 7. Below 50°C, $\langle P_4 \rangle_{mp}$ is negative, which corresponds to the minimum in the yielding region. At 50°C, $\langle P_4 \rangle_{mp}$shows an abrupt jump, and then remains about zero above 50°C because $\langle P_4 \rangle$ monotonously increases with strain. The transition temperature of 50°C coincides with the disappearance of heterogeneous load sharing (shown in Fig. 5) at the transition from the leather-like region to the α_1 relaxation region. Because the minimum in $\langle P_4 \rangle$ can be explained by steric hindrance of bulky lamellar cluster units [23], the existence of the minimum suggests that the molecular orientation is rather hindered in the leather-like region. For the crystalline phase, although intercrystalline motion is frozen in the leather-like region, molecular orientation would be smooth in the α_1 relaxation region because intercrystalline motion is activated. The orientational behavior in the strain-hardening region is shown in Fig. 8, where the values of $\langle P_2 \rangle$ and $\langle P_4 \rangle$ at $\varepsilon = 10$ are plotted against temperature. Because the values of $\langle P_2 \rangle$ and $\langle P_4 \rangle$ at $\varepsilon = 10$ increase with temperature and the slopes become steeper at 50°C, higher orientation toward the draw direction is achieved in the α relaxation region. The enhancement of the molecular orientation in the α_1 relaxation region is also understood by the activated intercrystalline relaxation [5].

The peculiar orientational behavior in the cold drawing of PE is visualized by the orientation distribution functions in Fig. 9. Above 50°C, $N(\theta)$ at the second yield point

has a prominent peak at θ = 0°, which means molecular orientation is essentially along the draw direction. However, at 20°C, $N(\theta)$ at the second yield point has a broad maximum at an intermediate angle (30–70°) from the drawing direction, suggesting that orientation is hindered by the rigid lamellar cluster units [23] only in the leather-like region.

The microscopic structural changes during hot drawing of HDPE have been intensively investigated by Men and coworkers [9,37,38]. They have reported the effect of the drawing temperature and the lamellar thickness on the void formation. According to their results [38], the void formation in the present sample (the lamellar thickness of ~17 nm) is expected to occur below 50°C. The agreement with the transition temperature of the microscopic stress and orientational behaviors implies that the deformation mechanism is influenced by whether the voids form or not.

4. Conclusion

The microscopic structural changes of HDPE during hot drawing were observed by *in situ* Raman spectroscopy. In the leather-like region, $\Delta\nu_s$ sharply increased, while $\Delta\nu_{as}$ monotonously decreased in the yielding region, which indicates that load sharing on the crystalline chain was heterogeneous. The microscopic stress decreased with increasing temperature, and the stress on the crystalline chain almost disappeared in the α_1 relaxation region. The orientation owing to elongation was greatly enhanced at elevated temperatures. While $N(\theta)$ had a broad maximum at an intermediate angle (θ = 30–70°) in the leather-like region, $N(\theta)$ always had a maximum in the draw direction in the α_1 relaxation region. These microscopic stress and orientational behaviors were explained by the increase of mobility of bulky lamellar cluster units because of intercrystalline

relaxation.

Acknowledgments

The temperature-controlled tensile machine for microscopy was kindly lent by Japan High Tech Co. Ltd. YH is thankful for financial support from the Japanese Society for the Promotion of Science KAKENHI (Grant number 26410221).

References

[1] N. McCrum, B. Read, G. Williams, Anelastic and dielectric effects in polymeric solids, WILEY, 1967.

[2] R. Boyd, Relaxation processes in crystalline polymers: experimental behaviour—a review, Polymer. 26 (1985) 323–347.

[3] R. Boyd, Relaxation processes in crystalline polymers: molecular interpretation—a review, Polymer. 26 (1985) 1123–1133.

[4] H. Nakayasu, H. Markovitz, D.J. Plazek, The Frequency and Temperature Dependence of the Dynamic Mechanical Properties of a High Density Polyethylene, J. Rheol. (N. Y. N. Y). 5 (1961) 261.

[5] M. Takayanagi, Some morphological factors in thermomechanical analysis of crystalline polymers, J. Macromol. Sci. Part B. 9 (1974) 391–433.

[6] Y. Men, J. Rieger, H.-F. Endeler, D. Lilge, Mechanical α-Process in Polyethylene, Macromolecules. 36 (2003) 4689–4691.

[7] M. Sharpe, Polymer ultradrawability: the crucial role of α-relaxation chain mobility in the crystallites, J. Environ. Monit. 50 (1999) 271–285.

[8] H. Zhou, G. Wilkes, Orientation anisotropy of the mechanical α relaxation of high-density polyethylene films having a well-defined stacked lamellar morphology, Macromolecules. 30 (1997) 2412–2421.

[9] Z. Jiang, Y. Tang, J. Rieger, H.-F. Enderle, D. Lilge, S. V. Roth, et al., Structural evolution of tensile deformed high-density polyethylene at elevated temperatures: Scanning synchrotron small- and wide-angle X-ray scattering studies, Polymer. 50 (2009) 4101–4111.

[10] B. Read, R. Stein, Polarized infrared studies of amorphous orientation in polyethylene and some ethylene copolymers, Macromolecules. 1 (1968) 116–126.

[11] U. Hoffmann, F. Pfeifer, S. Okretic, Rheo-optical Fourier transform infrared and Raman spectroscopy of polymers, Appl. Spectrosc. 47 (1993) 1531–1539.

[12] W. Glenz, A. Peterlin, Infrared studies of drawn polyethylene. II. Orientation behavior of highly drawn linear and ethyl‐branched polyethylene, J. Polym. Sci. Part A−2. 9 (1971) 1191–1217.

[13] N. Everall, J. Chalmers, P. Mills, Use of polarized resonance Raman spectroscopy of a polyene probe, and FT-IR dichroism, to probe amorphous-phase orientation in uniaxially drawn poly (ethylene), Appl. Spectrosc. 50 (1996) 1229–1234.

[14] H. Li, W. Zhou, Y. Ji, Z. Hong, B. Miao, X. Li, et al., Spatial distribution of crystal orientation in neck propagation: An in-situ microscopic infrared imaging study on polyethylene, Polymer. 54 (2013) 972–979.

[15] P. Lapersonne, D. Bower, I. Ward, Molecular orientation and conformational changes due to uniaxial-planar deformation of Poly (ethylene terephthalate) films, Polymer. 33 (1992) 1277–1283.

[16] Neil Everall, P.R. Griffiths, J.M. Chalmers, Vibrational Spectroscopy of Polymers: Principles and Practice, 2007.

[17] R.P. Wool, R.S. Bretzlaff, Infrared and Raman Spectroscopy of Stressed Polyethylene, J. Polym. Sci. Part B Polym. Phys. 24 (1986) 1039–1066.

[18] D.I. Bower, INVESTIGATION OF MOLECULAR ORIENTATION DISTRIBUTION BY POLARIZED RAMAN SCATTERING AND

POLARIZED FLUORESCENCE, J. Polym. Sci. PartA-2, Polym. Phys. 10 (1972) 2135–2153.

[19] D.I. Bower, ORIENTATION DISTRIBUTION FUNCTION FOR UNIAXIALLY ORIENTED POLYMERS, J. Polym. Sci. PartA-2, Polym. Phys. 19 (1981) 93–107.

[20] M. Richard-Lacroix, C. Pellerin, Accurate New Method for Molecular Orientation Quantification Using Polarized Raman Spectroscopy, Macromolecules. 46 (2013) 5561–5569.

[21] M. Tanaka, R.J. Young, Review Polarised Raman spectroscopy for the study of molecular orientation distributions in polymers, J. Mater. Sci. 41 (2006) 963–991.

[22] J. Brundrup, E.H. Immergut, E.A. Grulke, A. Abe, D.R. Bloch, Polymer Handbook, 4th ed., WILEY, 1999.

[23] T. Kida, T. Oku, Y. Hiejima, K. Nitta, Deformation mechanism of high-density polyethylene probed by in situ Raman spectroscopy, Polyme. 58 (2015) 88–95.

[24] M. Gall, P. Hendra, C. Peacock, Laser-Raman spectrum of polyethylene: Part 1. Structure and analysis of the polymer, Polymer. 13 (1972) 104–108.

[25] M. Gall, P. Hendra, O. Peacock, M.E.A. Cudby, H.A. Willis, The laser-Raman spectrum of polyethylene: The assignment of the spectrum to fundamental modes of vibration, Spectrochim. Acta Part A Mol. Spectrosc. 28A (1972) 1485–1496.

[26] D.V. Luu, L. Cambon, C. Lapeyre, Caracterisation des Phases dans le Polyethylene par Effet Raman, J. Raman Spectrosc. 9 (1980) 172–175.

[27] G. Strobl, W. Hagedorn, Raman spectroscopic method for determining the crystallinity of polyethylene, J. Polym. Sci. Polym. Phys. Ed. 16 (1978) 1181–1193.

[28] S Frisk, R.M. Ikeda, D.B. Chase, J.F. Rabolt, Determination of the Molecular Orientation of Poly(propylene terephthalate) Fibers Using Polarized Raman Spectroscopy: A Comparison Methods, Appl. Spectrosc. 58 (2004) 279–286.

[29] M.J. Citra, D.B. Chase, R.M. Ikeda, K.H. Gardner, Molecular Orientation of High-Density Polyethylene Fibers Characterized by Polarized Raman Spectroscopy, Macromolecules. 28 (1995) 4007–4012.

[30] M. Pigeon, R. E, Prud'homme, M. Pezolet, Characterization of molecular orientation in polyethylene by Raman spectroscopy, Macromolecules. 24 (1991) 5687–5694.

[31] K.-H. Nitta, M. Takayanagi, Direct observation of the deformation of isolated huge spherulites in isotactic polypropylene, J. Mater. Sci. 38 (2003) 4889–4894.

[32] K.-H. Nitta, M. Takayanagi, Application of Catastrophe Theory to the Neck-initiation of Semicrystalline Polymers Induced by the Intercluster Links, Polym. J. 38 (2006) 757–766.

[33] K.-H. Nitta, M. Takayanagi, Novel Proposal of Lamellar Clustering Process for Elucidation of Tensile Yield Behavior of Linear Polyethylenes, J. Macromol. Sci. Part B Phys. 42 (2003) 107–126.

[34] M. Kuriyagawa, K.-H. Nitta, Structural explanation on natural drawratio of metallocene-catalyzed high density polyethylene, Polymer (Guildf). 52 (2011) 3469–3477.

[35] I.M. Ward, J. Sweeney, Mechanical Properties of Solid Polymers, 3rd ed., WILEY, 2013.

[36] K.-H. Nitta, N. Yamaguchi, Influence of Morphological Factors on Tensile Properties in the Pre-yield Region of Isotactic Polypropylenes, Polym. J. 38 (2006) 122–131.

[37] Y. Men, J. Rieger, G. Strobl, Role of the entangled amorphous network in tensile deformation of semicrystalline polymers., Phys. Rev. Lett. 91 (2003) 095502.

[38] Y. Wang, Z. Jiang, L. Fu, Y. Lu, Y. Men, Lamellar thickness and stretching temperature dependency of cavitation in semicrystalline polymers., PLoS One. 9 (2014) e97234.

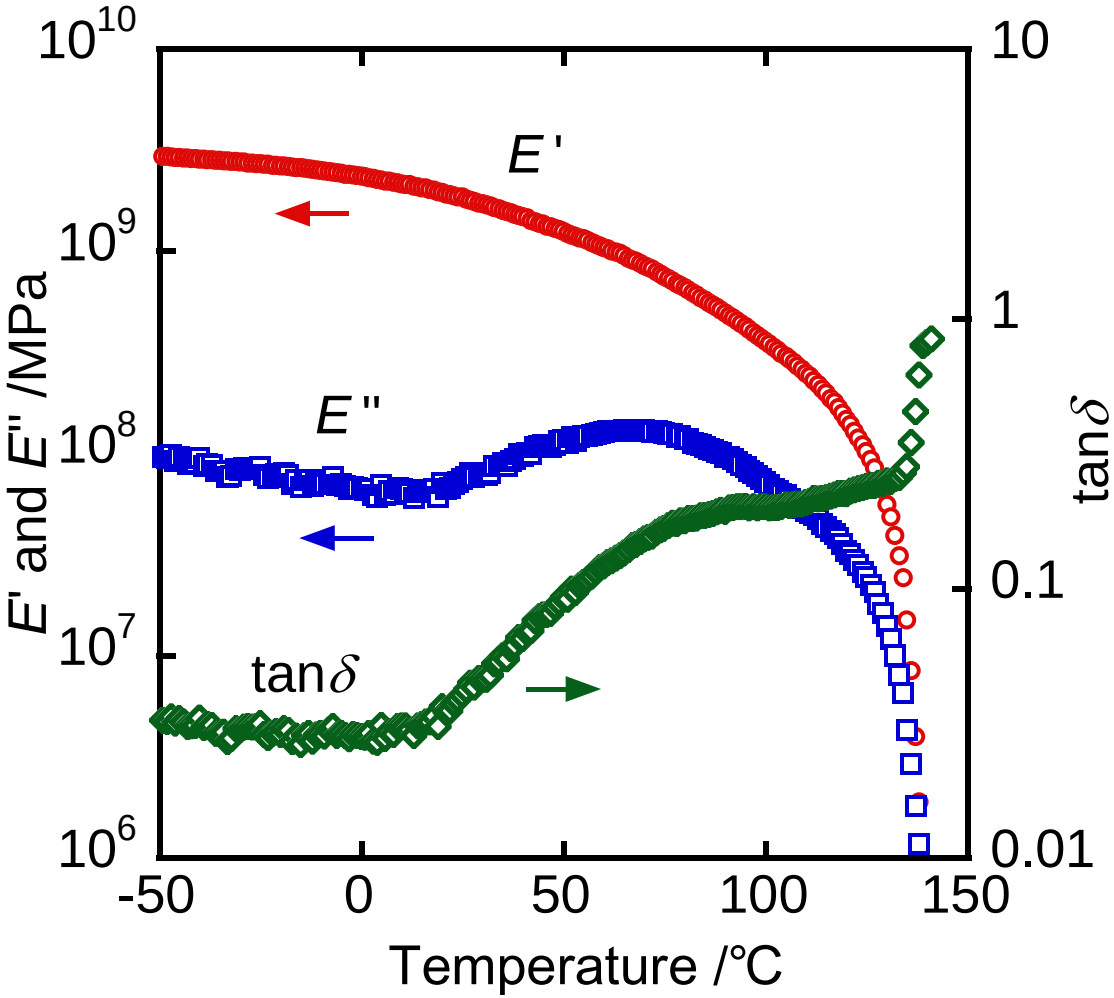

Fig.1 Dynamic mechanical spectra of HDPE at constant frequency of 10 Hz.

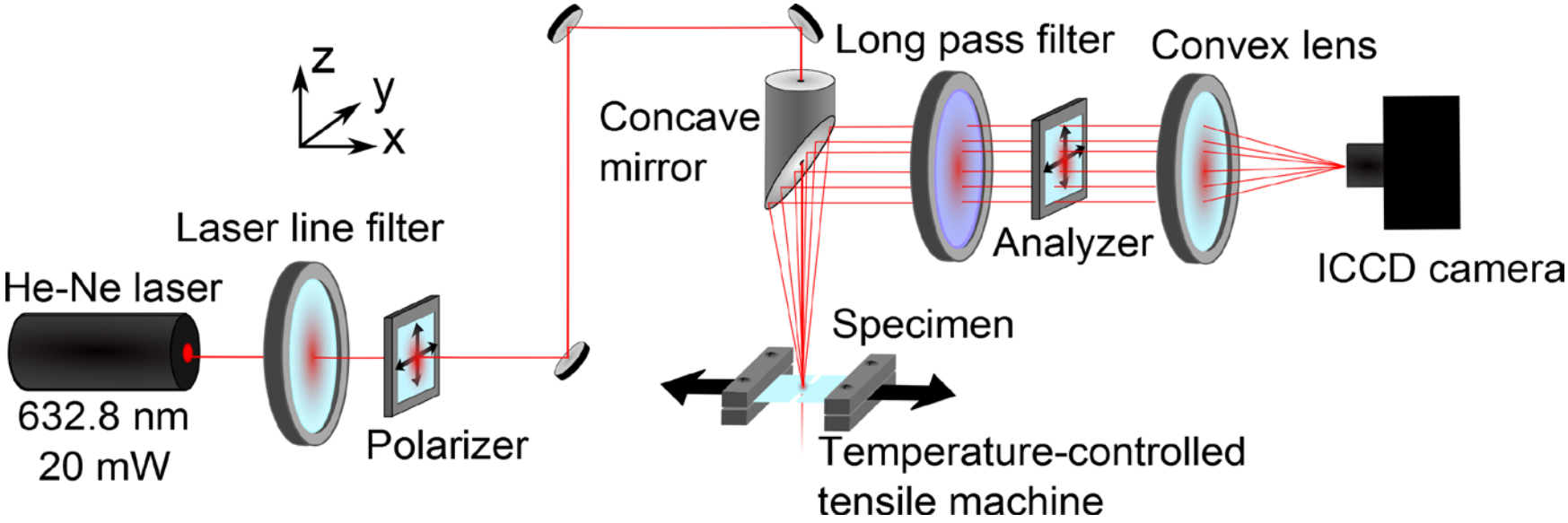

Fig.2 Schematic illustration of rheo-optical system for *in situ* Raman spectroscopy.

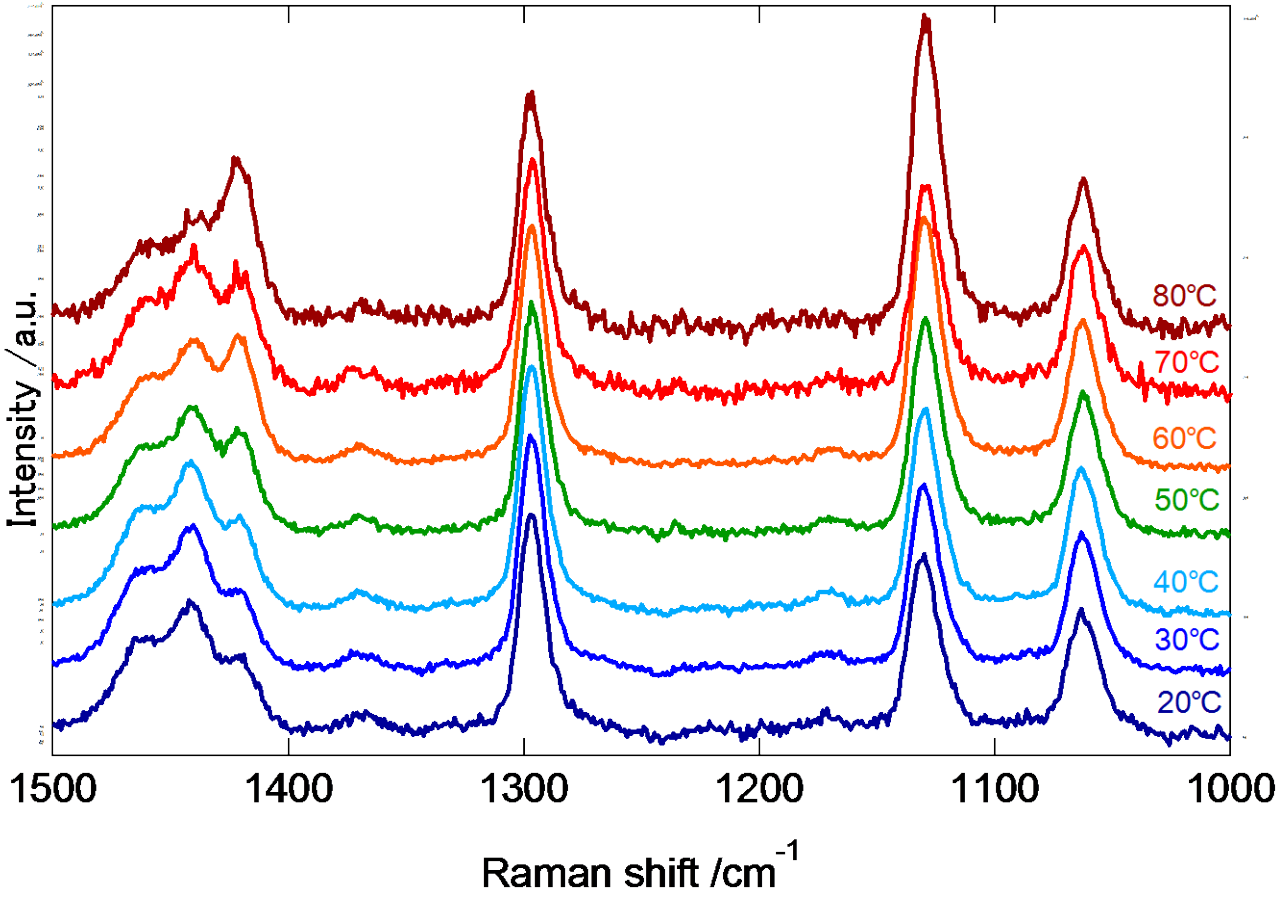

Fig.3 *In situ* Raman spectra of HDPE at ε=10. The drawing temperature is attached at each spectrum.

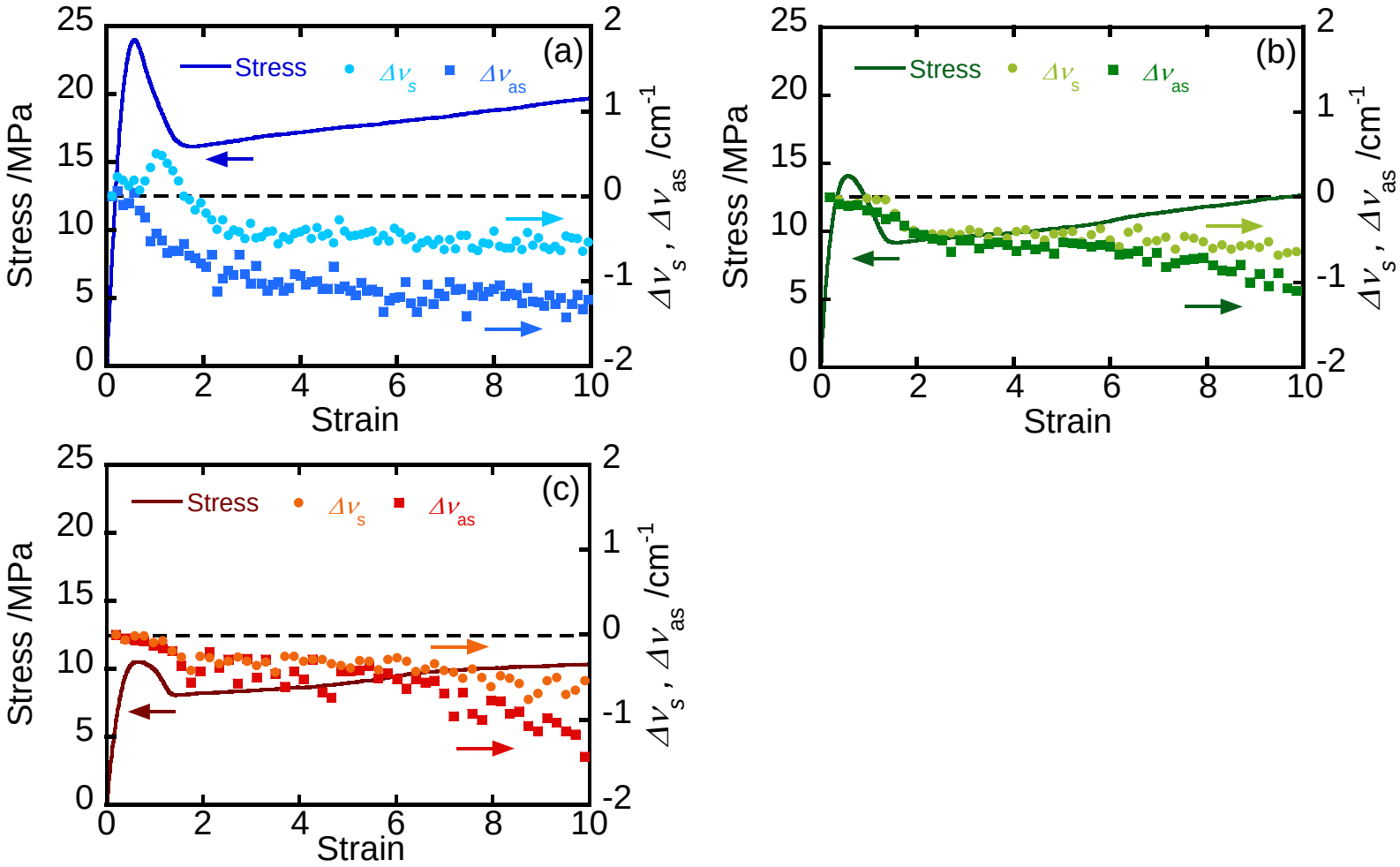

Fig.4 Strain dependences of stress and peak shifts $\Delta\nu_s$ (circles) and $\Delta\nu_{as}$ (squares) of HDPE at (a) 20 °C, (b) 50 °C and (c) 80 °C.

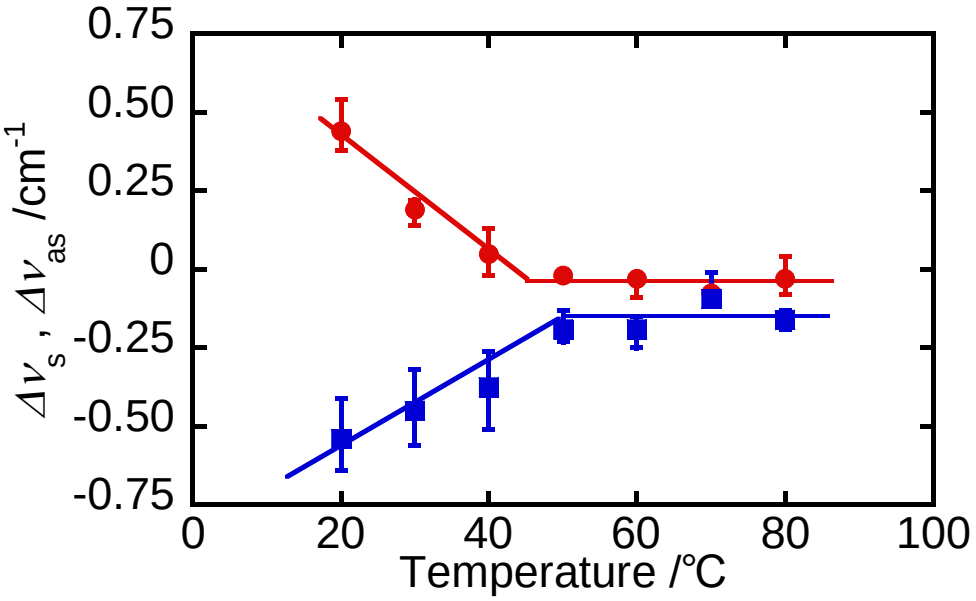

Fig.5 Temperature dependences of peak shifts $\Delta\nu_s$ (circles) and $\Delta\nu_{as}$ (squares) at the second yield point ($\varepsilon = 1.1$).

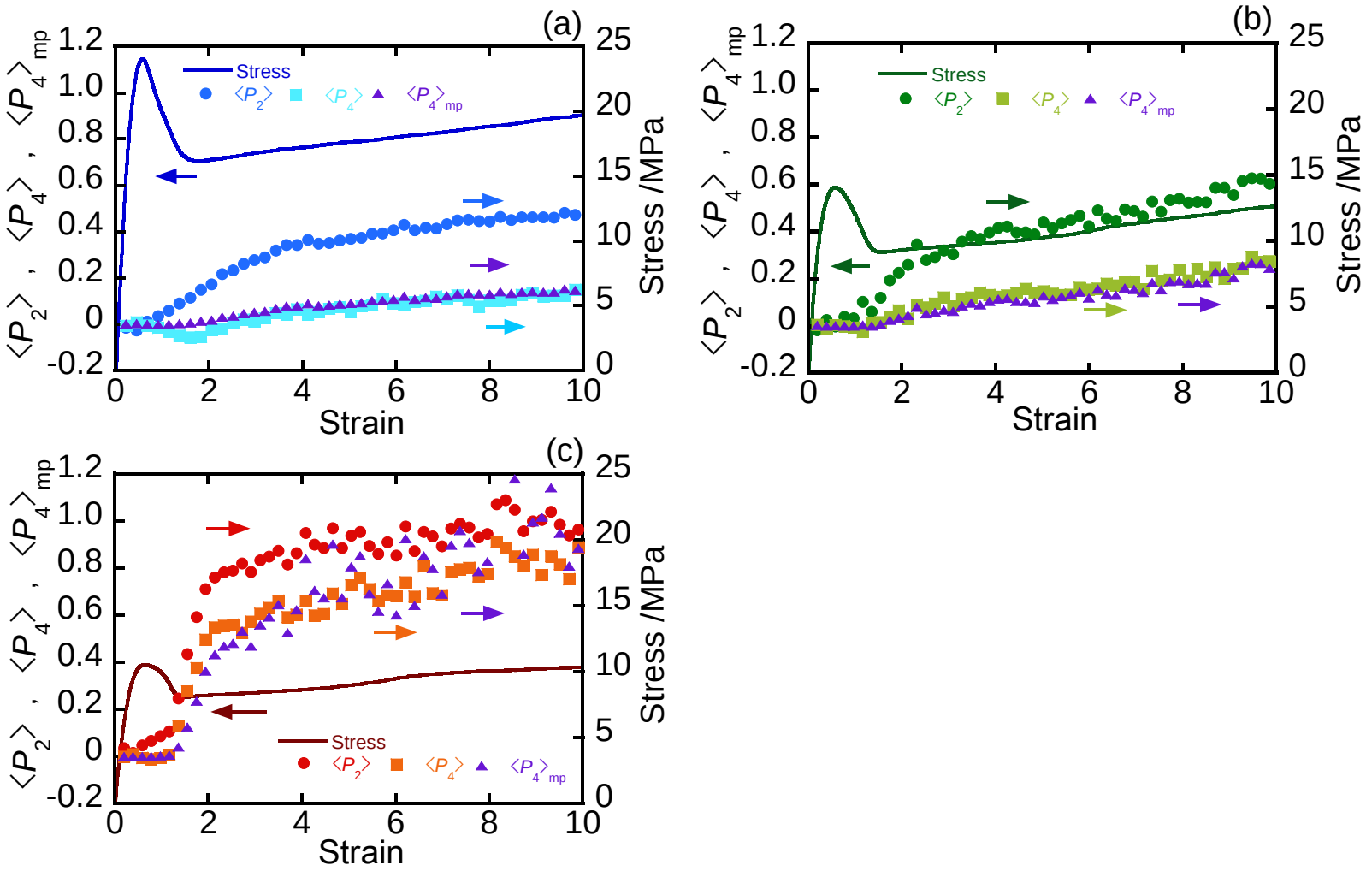

Fig.6 Strain dependences of orientation parameters $\langle P_2 \rangle$ (circles), $\langle P_4 \rangle$ (squares) and $\langle P_4 \rangle_{mp}$ (triangles) at (a) 20 °C, (b) 50 °C and (c) 80 °C. Stress-strain curves are also shown.

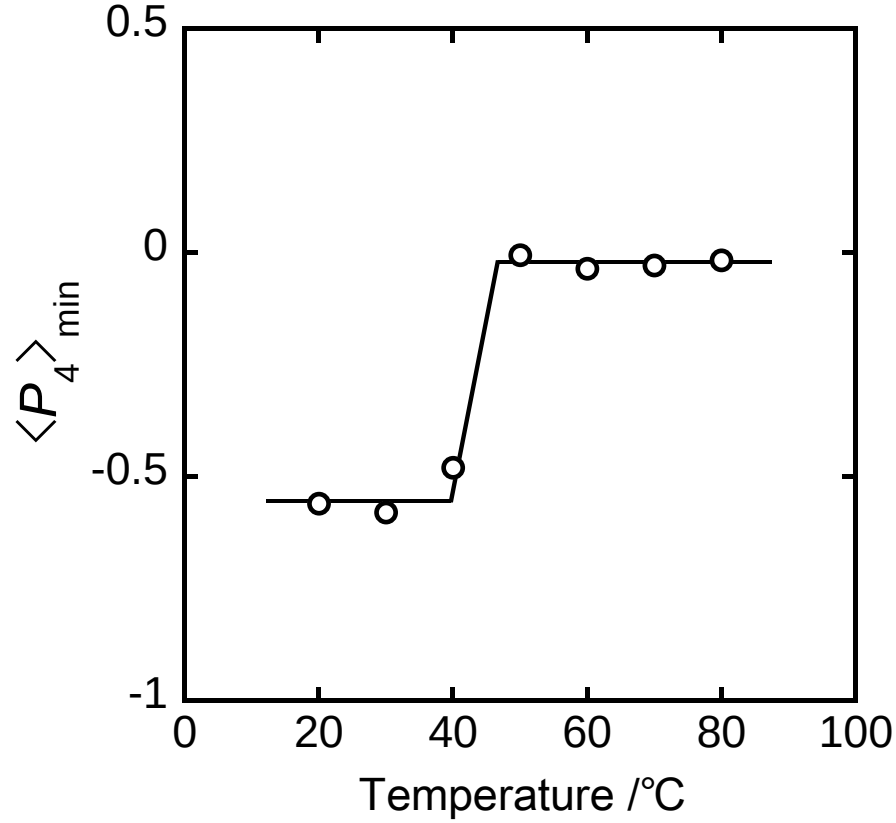

Fig.7 Temperature dependence of the minimum value of $\langle P_4 \rangle$ during elongation ($\langle P_4 \rangle_{\mathrm{min}}$).

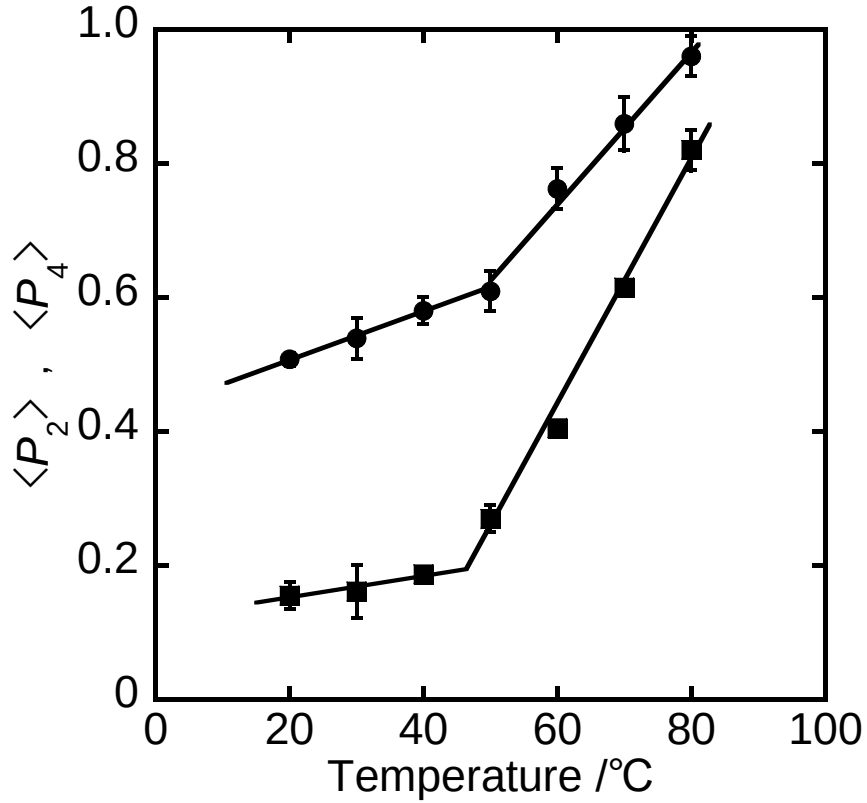

Fig.8 Temperature dependences of orientation parameters $\langle P_2 \rangle$ (circles) and $\langle P_4 \rangle$ (squares) at $\varepsilon = 10$.

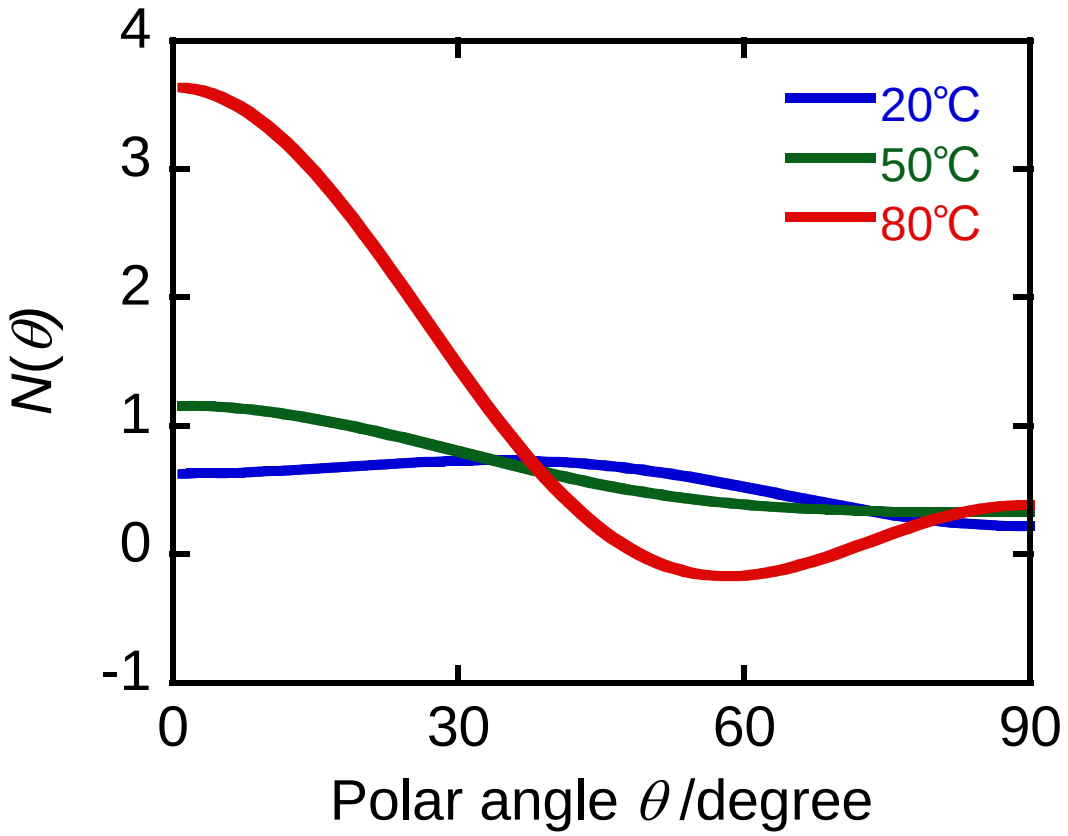

Fig.9 Orientation distribution functions $N(\theta)$ at the second yield point at (a) 20 °C, (b) 50 °C and (c) 80 °C.

Table 1 Vibrational and phase assignments of the Raman spectrum of polyethylene [21–24].

Raman shift (cm^{-1})	Mode[a]	Phase	Type of symmetry
1063	ν_{as} (C–C)	Trans chain	$B_{2g} + B_{3g}$
1130	ν_{s} (C–C)	Trans chain	$A_g + B_{1g}$
1298	ν_{t} (CH_2)	Crystalline	$B_{2g} + B_{3g}$
1418	δ (CH_2)	Crystalline	A_g
1440	δ (CH_2)	Trans chain (interphase)	$A_g + B_{1g}$
1461	δ (CH_2)	Amorphous	$A_g + B_{1g}$

[a] ν_{as} = anti-symmetric stretching; ν_{s} = symmetric stretching; ν_{t} = twisting; δ = bending)